Eur. Phys. J. D **41**, 589–598 (2007)
DOI: 10.1140/epjd/e2006-00265-1

THE EUROPEAN PHYSICAL JOURNAL D

Maximum confidence measurements and their optical implementation

S. Croke[1,2,a], P.J. Mosley[3], S.M. Barnett[1], and I.A. Walmsley[3]

[1] Department of Physics, University of Strathclyde, Glasgow G4 0NG, UK
[2] Department of Mathematics, University of Glasgow, Glasgow G12 8QW, UK
[3] Clarendon Laboratory, Oxford University, Parks Road, Oxford, OX1 3PU, UK

Received 19 June 2006 / Received in final form 5 October 2006
Published online 8 December 2006 –

Abstract. Perfect discrimination between non-orthogonal states is forbidden by the laws of quantum mechanics. Several strategies to discriminate optimally between states of an arbitrary set exist, and many of these have been implemented in experiments using optical polarisation. In this paper we discuss maximum confidence measurements and their recent optical implementation.

PACS. 42.50.Xa Optical tests of quantum theory – 03.67.Hk Quantum information

1 Introduction

In classical mechanics, a system is described by variables such as position and momentum, which can in principle be measured arbitrarily accurately to obtain complete information about the state of the system. Thus, when classical systems are used to carry information, it is possible, at least in theory, to distinguish perfectly between any given set of signal states, although in reality a noisy signal may make this impracticable. In quantum mechanics however, the state of a system is not itself an observable. Furthermore, the act of measuring a quantum system changes the state, destroying the information previously contained therein. As a consequence, the accuracy with which it is possible to discriminate between states of an arbitrary set is limited by fundamental laws of quantum mechanics.

Perfect discrimination is possible only when the signal states form a mutually orthogonal set. However, there are certain advantages to be gained in exploiting quantum effects arising from the use of non-orthogonal signal states. For example, cryptographic protocols using non-orthogonal states are provably secure against attack by eavesdroppers [1,2]. Also, the information carrying capability for certain noisy channels is maximised by using non-orthogonal states [3]. It is important therefore, to understand how to discriminate optimally between states of an arbitrary set [4]. Optimality, of course, lies in the eye of the beholder. It requires a criterion against which the system performance can be judged. For example, is it worse to get a wrong answer or miss a right one? Possibly the simplest definition of optimality is a measurement which minimises the probability of incorrectly identifying the state [5–7]. However, error-free or unambiguous discrimination is possible between two non-orthogonal states, if we are prepared to accept the possibility of an inconclusive result [8]. This strategy can be extended to larger numbers of states [9], but is only applicable to linearly independent sets [10]. It has recently been shown however, that an analogous strategy — one which achieves maximum confidence that when a state is identified it was indeed present — is possible for linearly dependent states [11]. Other definitions of optimal outcomes include maximising the mutual information shared by the receiving and transmitting parties [12,13], and maximising the fidelity between the state received and one transmitted on the basis of the measurement result [14,15] as well as minimising the a posteriori probability of error [16]. Variants on the quantum state discrimination problem have also been considered, including assigning the state of a system to one of two complementary subsets of a set of non-orthogonal states [17], and the special case where one of the subsets contains a single state, known as quantum state filtration [17–19].

Experimental demonstrations of optimal strategies to date have predominantly used the polarisation state of light as a two-level system or qubit [20]. This is largely due to the relative ease with which polarisation states can be created and manipulated in the laboratory using readily available linear optical components. One alternative is the construction of a multi-level optical system by making use of different ports of a multi-rail interferometer [18]. This approach, which also uses linear optical elements to manipulate input states, was used to demonstrate unambiguous discrimination between three non-orthogonal states, and between a pure and a mixed state in three dimensions [21]. Examples of optimal minimum

[a] e-mail: sarah@phys.strath.ac.uk

error, mutual information, and unambiguous discrimination measurement strategies have been demonstrated in experiments on optical polarisation [22–26]. We have recently implemented a maximum confidence measurement between three equiprobable symmetric qubit states in this way [27]. In this paper we will discuss maximum confidence measurements and their optical implementation. The remainder of the paper is organised as follows. In Section 2 we discuss how the maximum confidence measurement is constructed, and compare it to other strategies. In Section 3 we present our experimental design and its implementation. We discuss the experimental results and sources of error in Section 4, before concluding in Section 5.

2 Maximum confidence measurements

In quantum state discrimination, it is usually assumed that both the set of possible states $\{\hat{\rho}_i\}$, and the a priori probabilities $\{p_i\}$ that each state is prepared are known, although this is not always the case [28]. The problem then is to choose the measurement to determine best which state was actually prepared. A conventional, von Neumann measurement gives outcomes corresponding to one of a set of mutually orthogonal states. The number of outcomes is therefore restricted by the dimensions of the state space of the system. More general measurements are possible however, and any measurement in quantum mechanics can be described mathematically by a probability operator measure (POM) [5], also known as a positive operator valued measure [29]. Thus the optimisation can be cast as a purely mathematical problem whose convex nature allows globally optimal solutions to be found. In the POM formalism, measurement results $\{\omega_i\}$ are associated with operators $\{\hat{\Pi}_i\}$, which completely specify the measurement. The operator $\hat{\Pi}_j$ is defined by the probability of occurence of the associated measurement result

$$P(\omega_j|\hat{\rho}) = \mathrm{Tr}(\hat{\rho}\hat{\Pi}_j) \tag{1}$$

for a measurement on a system in state $\hat{\rho}$. In order to form a physically realisable measurement, these operators must be non-negative, and satisfy a completeness condition:

$$\hat{\Pi}_i \geq 0, \quad \sum_i \hat{\Pi}_i = \hat{\mathrm{I}}. \tag{2}$$

Although in general the result of a measurement will not reveal with certainty which state was prepared, it does provide information which allows us to modify our description of the state via Bayes' rule. Thus if outcome ω_j is obtained, the probability distribution for the input states $\{\hat{\rho}_i\}$ becomes:

$$P(\hat{\rho}_i|\omega_j) = \frac{P(\hat{\rho}_i)P(\omega_j|\hat{\rho}_i)}{P(\omega_j)} = \frac{p_i\mathrm{Tr}(\hat{\rho}_i\hat{\Pi}_j)}{\mathrm{Tr}(\hat{\rho}\hat{\Pi}_j)} \tag{3}$$

where $\hat{\rho} = \sum_i p_i\hat{\rho}_i$. Thus this represents the information we now have about the state *given* knowledge of the measurement result ω_j. It is usual to associate each input state with a particular measurement result, so that when result ω_j is obtained, we take this to imply that the state of the system was $\hat{\rho}_j$. The probability that we are correct to do so is the quantity

$$P(\hat{\rho}_j|\omega_j) = \frac{p_j\mathrm{Tr}(\hat{\rho}_j\hat{\Pi}_j)}{\mathrm{Tr}(\hat{\rho}\hat{\Pi}_j)}, \tag{4}$$

and is maximised by the maximum confidence measurement. This conditional probability is therefore interpreted as our confidence in identifying state $\hat{\rho}_j$ as a result of obtaining outcome ω_j. Before discussing how the maximum confidence measurement is constructed, it is worth commenting that, having identified this conditional probability as a quantity of interest, there are still several optimality conditions which may be applied to form distinct measurement strategies. Note that the average of this quantity, over all measurement outcomes, is given by:

$$P_{corr} = \sum_j P(\omega_j)P(\hat{\rho}_j|\omega_j) = \sum_j P(\hat{\rho}_j)P(\omega_j|\hat{\rho}_j), \tag{5}$$

and represents the overall probability of correctly identifying the state, the figure of merit maximised by the minimum error measurement. Another possibility is to maximise the smallest value of $P(\hat{\rho}_j|\omega_j)$ for a given set of states, i.e. apply a worst-case optimality condition [16]. The maximum confidence measurement however, optimises this probability for each state in a set independently. Thus, for each input state $\hat{\rho}_j$, we look for the positive operator $\hat{\Pi}_j$ which maximises the conditional probability in equation (4). The operators $\{\hat{\Pi}_j\}$ are treated as independent, essentially relaxing the completeness condition in equation (2). The result of this is that ultimately an inconclusive outcome may be needed in order to form a physically realisable measurement, but the remaining outcomes each achieve the maximum possible value of $P(\hat{\rho}_j|\omega_j)$ for the corresponding state $\hat{\rho}_j$. Thus whenever outcome ω_j is obtained, we can be as confident as possible that $\hat{\rho}_j$ was indeed prepared. Note that as the operator $\hat{\Pi}_j$ appears in the denominator and the numerator, it can only be determined up to an arbitrary multiplicative factor. These factors can always be chosen such that $\hat{\Pi}_? \geq 0$, where

$$\hat{\Pi}_? = \hat{\mathrm{I}} - \sum_j \hat{\Pi}_j \tag{6}$$

is the POM element corresponding to the inconclusive result. Thus the problem is reduced to finding the positive operator $\hat{\Pi}_j$ which maximises the right hand side of equation (4).

As pointed out in [11], a closed-form solution for an arbitrary set of states is made possible by the ansatz:

$$\hat{\Pi}_j = c_j\hat{\rho}^{-1/2}\hat{Q}_j\hat{\rho}^{-1/2}, \tag{7}$$

where $\hat{Q}_j$ is a positive operator with unit trace, and hence c_j represents the probability of occurrence of outcome ω_j, $c_j = P(\omega_j)$. With this definition equation (4) becomes

$$\begin{aligned} P(\hat{\rho}_j|\omega_j) &= p_j\mathrm{Tr}(\hat{\rho}^{-1/2}\hat{\rho}_j\hat{\rho}^{-1/2}\hat{Q}_j) \\ &= p_j\mathrm{Tr}(\hat{\rho}_j\hat{\rho}^{-1})\mathrm{Tr}(\hat{\rho}'_j\hat{Q}_j) \end{aligned} \tag{8}$$

where $\hat{\rho}'_j = \hat{\rho}^{-1/2}\hat{\rho}_j\hat{\rho}^{-1/2}/\mathrm{Tr}(\hat{\rho}_j\hat{\rho}^{-1})$. $\hat{\rho}'_j$ and $\hat{Q}_j$ are both positive, trace-1 operators, and thus can be thought of as density operators. $P(\hat{\rho}_j|\omega_j)$ is therefore maximised if $\hat{Q}_j$ corresponds to the state with which $\hat{\rho}'_j$ has largest overlap, i.e. is a projector onto the pure state

$$\hat{Q}_j = |\lambda'^{max}_j\rangle\langle\lambda'^{max}_j|, \tag{9}$$

where $|\lambda'^{max}_j\rangle$ is the eigenket of $\hat{\rho}'_j$ corresponding to its largest eigenvalue λ'^{max}_j. The limit is then given by

$$[P(\hat{\rho}_j|\omega_j)]_{max} = p_j\mathrm{Tr}(\hat{\rho}_j\hat{\rho}^{-1})\lambda'^{max}_j. \tag{10}$$

We can also easily find the corresponding POM element by applying the transformation in equation (7):

$$\hat{\Pi}_j = c_j\hat{\rho}^{-1/2}|\lambda'^{max}_j\rangle\langle\lambda'^{max}_j|\hat{\rho}^{-1/2}. \tag{11}$$

If the state $\hat{\rho}_j$ is pure then this simplifies to

$$\hat{\Pi}_j \propto \hat{\rho}^{-1}\hat{\rho}_j\hat{\rho}^{-1}. \tag{12}$$

Although the optimal measurement is not uniquely defined — some arbitrariness remains in the choice of constants of proportionality — the maximum confidence strategy is completely specified by the above. The strategy is defined by the criterion that whenever we identify state $\hat{\rho}_j$, we do so as confidently as is possible. The fact that it is always possible to construct a measurement which achieves this maximum confidence for each state in a given set is precisely because the optimality of the POM elements is independent of their respective weights. Furthermore, as the elements are treated completely independently in the derivation it is clear that the optimality of a given element $\hat{\Pi}_j$ is independent of how we choose to construct the other elements in the POM to satisfy the completeness relation. Consider therefore the quantum state filtration problem — the question of whether the system is in state $\hat{\rho}_j$ or simply any one of the other possible states $\{\hat{\rho}_i\}, i \neq j$. This may seem less demanding than the problem of discriminating between all the states equally. Indeed in the minimum error approach, the probability of making an error in the filtration problem can be smaller than that in the corresponding discrimination problem [17]. It is clear from the argument above however, that in the maximum confidence approach, the confidence in identifying state $\hat{\rho}_j$ cannot be increased by considering this more restrictive problem. The limit in equation (10) is dependent only on the geometry of the set. In this sense the limit is a measure of how distinguishable $\hat{\rho}_j$ is in the given set.

If the states $\{\hat{\rho}_i\}$ are linearly independent, the limit is unity and the state can be distinguished without error. Thus unambiguous discrimination is an example of a maximum confidence measurement. In unambiguous discrimination the constants of proportionality c_j are often chosen to minimise the probability of occurrence of the inconclusive result, although this may not always be the most suitable criterion. For example, in the case of two non-orthogonal states, if the a priori probability of occurrence for one of the states is sufficiently small, the measurement which minimises the probability of obtaining the inconclusive result never identifies this state [30]. Thus if we wish to have at least some probability of identifying each state, we may be prepared to accept an inconclusive outcome which occurs more often than is strictly necessary. For a maximum confidence measurement to discriminate between states of an arbitrary set, we also need some other criteria to choose the constants of proportionality. In some cases, as with unambiguous discrimination, we may choose to minimise the probability of occurrence of the inconclusive outcome [11]. Indeed, for a linearly dependent set the number of operators $\hat{\Pi}_j$ will be greater than the dimensionality of the space spanned by the states, and it may be possible to choose the constants such that an inconclusive outcome is not necessary. However, it is interesting to note that, unlike unambiguous discrimination, the quantity $[P(\hat{\rho}_j|\omega_j)]_{max}$ will in general be different for different states $\hat{\rho}_j$. It may sometimes be useful to choose a measurement which only ever identifies the states for which this limit is greater than a certain threshold value. For example, it was pointed out by Sun et al. [18], that unambiguous discrimination is possible between a pure and a mixed state of a two-level system (we shall refer to these as $\hat{\rho}_{pure}$ and $\hat{\rho}_{mixed}$ respectively). This is achieved by a von Neumann measurement with outcomes corresponding to states along and orthogonal to $\hat{\rho}_{pure}$. The result corresponding to a measurement along $\hat{\rho}_{pure}$ is interpreted as inconclusive, while the result corresponding to the state orthogonal to $\hat{\rho}_{pure}$ tells us with certainty that the state was $\hat{\rho}_{mixed}$. Within the framework of maximum confidence measurements it is possible to construct a measurement which sometimes identifies $\hat{\rho}_{mixed}$ with certainty, sometimes identifies $\hat{\rho}_{pure}$ as confidently as possible, and sometimes gives an inconclusive result. However, although the probability of occurrence of the inconclusive result may be smaller in this case, we may wish to only allow unambiguous results, and thus choose the former. Therefore the question of how to construct a maximum confidence strategy which is optimal for a given situation is dependent on the situation and the information desired.

Finally in this section, we compare maximum confidence measurements and minimum error measurements. As already noted, the two strategies can be thought of as applying a different optimality condition to the same quantity — the conditional probability $P(\hat{\rho}_j|\omega_j)$. The minimum error measurement, however, optimises an average over all measurement outcomes, and the POM elements must always form a complete set (clearly there will never be an inconclusive outcome, as if this were the case the expression in equation (5) could be increased by the addition of a term of the form $P(\omega_?)P(\hat{\rho}_j|\omega_?)$). As a result, finding the optimal minimum error measurement is in general a difficult problem. In fact, although the necessary and sufficient conditions which the optimal measurement must satisfy are known [6,7], the measurement itself is known only in a limited number of special cases [5,7,31–34]. As we have seen, the maximum

confidence measurement will in general have an inconclusive outcome. In the special case where the maximum confidence is the same for all states in a set, and the POM elements in equation (11) form a complete set, it may be seen that the two strategies coincide. More generally, it is clear from examination of equation (5) that a limit to this quantity is given by the largest value of the maximum confidence for a given set.

In certain symmetric cases the square root measurement [31,35], given by

$$\hat{\Pi}_j = p_j \hat{\rho}^{-1/2} \hat{\rho}_j \hat{\rho}^{-1/2}, \tag{13}$$

is the optimal minimum error measurement. Interestingly, the maximum confidence POM elements have a similar form to the above, but the square root measurement has the advantage that it is always possible to form a POM from these elements as

$$\sum_j \hat{\Pi}_j = \hat{\rho}^{-1/2} \hat{\rho} \hat{\rho}^{-1/2} = \hat{\mathrm{I}}. \tag{14}$$

It has proved useful, in the absence of a general formula for the minimum error POM to investigate what information such a measurement can provide about a system in one of the states $\{\hat{\rho}_j\}$. Indeed this measurement is considered a 'pretty good' measurement even in cases where it is not optimal [34,35]. As the maximum confidence POM elements will not always form a complete measurement, elements of this form cannot in general be applied to the minimum error problem. The exception is when $\hat{\rho} \propto \hat{\mathrm{I}}$, and the states are all pure, in which case the square root measurement and the maximum confidence measurement coincide.

3 Experimental design

3.1 Outline of experiment

Our experiment was designed to discriminate with maximum confidence between three equiprobable ($p_i = 1/3, i = 0,1,2$) symmetric polarisation states given by $\hat{\rho}_i = |\Psi_i\rangle\langle\Psi_i|$ where

$$\begin{aligned} |\Psi_0\rangle &= \cos\theta|R\rangle + \sin\theta|L\rangle, \\ |\Psi_1\rangle &= \cos\theta|R\rangle + e^{2\pi i/3}\sin\theta|L\rangle, \\ |\Psi_2\rangle &= \cos\theta|R\rangle + e^{-2\pi i/3}\sin\theta|L\rangle, \end{aligned} \tag{15}$$

and $|R\rangle, |L\rangle$ denote right and left circular polarisation states respectively. This example was considered in [11] for a general two-level system with orthonormal base kets $|0\rangle, |1\rangle$. For our choice of $|R\rangle, |L\rangle$ as basis states, the input states correspond to elliptical polarisations lying on the same latitude of the Poincaré sphere [36] (see Fig. 1). In terms of the horizontal and vertical polarisations ($|H\rangle, |V\rangle$), we define $|R\rangle = (i|H\rangle + |V\rangle)/\sqrt{2}$, $|L\rangle = (|H\rangle + i|V\rangle)/\sqrt{2}$.

We will first outline the optimal measurement, and then discuss how this measurement can be implemented optically. For this set the a priori density operator, $\hat{\rho} = \cos^2\theta|R\rangle\langle R| + \sin^2\theta|L\rangle\langle L|$, is diagonal in the $|R\rangle, |L\rangle$ basis, and it is straightforward to calculate the optimal POM elements using equation (12). Thus the POM elements achieving maximum confidence are given by $\hat{\Pi}_i \propto |\phi_i\rangle\langle\phi_i|$, where

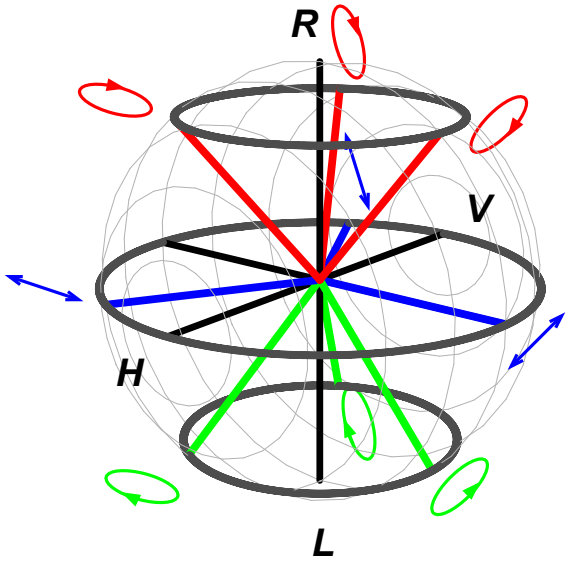

Fig. 1. (Colour online) Poincaré sphere representation of states. The north and south poles correspond to right (R) and left (L) circular polarisation respectively, while linear polarisations lie in the equatorial plane. The input states (red - lying in the northern hemisphere) and the states associated with the outcomes of the optimal maximum confidence (green - in the southern hemisphere) and minimum error (blue - on the equatorial plane) POMs are shown.

$$\begin{aligned} |\phi_0\rangle &= \sin\theta|R\rangle + \cos\theta|L\rangle, \\ |\phi_1\rangle &= \sin\theta|R\rangle + e^{2\pi i/3}\cos\theta|L\rangle, \\ |\phi_2\rangle &= \sin\theta|R\rangle + e^{-2\pi i/3}\cos\theta|L\rangle. \end{aligned} \tag{16}$$

The confidence that $\hat{\rho}_j$ was indeed present when outcome ω_j is obtained may then be written:

$$P(\hat{\rho}_j|\omega_j) = \frac{|\langle\phi_j|\Psi_j\rangle|^2}{\sum_i |\langle\phi_j|\Psi_i\rangle|^2}, \tag{17}$$

and has the value 2/3 for all $j = 0,1,2$. The states $|\phi_i\rangle$ are the reflection of the input states in the equatorial plane of the Poincaré sphere, and are shown in Figure 1. This corresponds to a measurement with outcomes associated with elliptical polarisations with opposite handedness to the input states.

Following [11], we choose the constants of proportionality such that the probability of occurence of the inconclusive result is minimised. Thus our optical apparatus was designed to implement the POM given by:

$$\begin{aligned} \hat{\Pi}_i &= (3\cos^2\theta)^{-1}|\phi_i\rangle\langle\phi_i|, \quad i = 0,1,2, \\ \hat{\Pi}_? &= (1 - \tan^2\theta)|R\rangle\langle R|, \end{aligned} \tag{18}$$

where $\hat{\Pi}_?$ denotes the POM element associated with the inconclusive result. The probability of obtaining this result is $P(?) = \cos 2\theta$. It can be seen that the inconclusive result is equally likely to occur for any of the input states, and thus gives no information about the state.

For comparison purposes, we note that the minimum error measurement for this set is given by the square root measurement discussed above, and may be written $\hat{\Pi}_i = (2/3)|\phi_i^{ME}\rangle\langle\phi_i^{ME}|$ where

$$
\begin{aligned}
|\phi_0^{ME}\rangle &= \frac{1}{\sqrt{2}}(|R\rangle + |L\rangle) \\
|\phi_1^{ME}\rangle &= \frac{1}{\sqrt{2}}(|R\rangle + e^{2\pi i/3}|L\rangle) \\
|\phi_2^{ME}\rangle &= \frac{1}{\sqrt{2}}(|R\rangle + e^{-2\pi i/3}|L\rangle). \qquad (19)
\end{aligned}
$$

These are the projections of the input states onto the equatorial plane of the Poincaré sphere, and are also shown in Figure 1. Thus the outcomes of this measurement are each associated with the linear polarisation specified by the orientation of the major axis of the polarisation ellipse of the corresponding input state. For this measurement the confidence figure of merit may be written in a similar form to that in equation (17) and is given by $(1 + \sin 2\theta)/3$ for all input states.

The optical network used to realise this measurement is shown in Figure 2. Quarter waveplates (QWP) and half waveplates (HWP) are used to perform unitary transformations, while polarising beamplitters (PBS) are used to separate orthogonal modes. POMs require an expansion of the Hilbert space beyond that of the states of interest [29]. The use of an interferometer in our set-up provides four orthogonal modes which can then be separated at PBS3-5 to realise a four outcome measurement. Note that the input states are states of a two-level system, and that the extra two orthogonal modes are provided by the vacuum input to PBS2, and it is this that provides the Naimark extension of the Hilbert space. The appropriate mixing of modes to perform the particular measurement we are interested in is achieved using HWP4-7 and QWP2-3.

Our design groups together the four outputs in pairs, so that two orthogonal modes in output arm A correspond to results $\omega_?, \omega_0$, while two in arm B correspond to results ω_1, ω_2. Thus the interferometer in our set-up performs the measurement described by the 2-element POM $\{\hat{\Pi}_? + \hat{\Pi}_0, \hat{\Pi}_1 + \hat{\Pi}_2\}$. The remaining unitary transformations and separation of modes necessary to perform the full four outcome measurement are performed by HWP7, QWP3 and PBS4-5. The photodetectors PD0-2,? measure the number of photons in the two orthogonal modes $\{H, V\}$ incident on each detector. As one of these modes is always empty, the detectors realise the projectors $\hat{\pi}_i = |H_i\rangle\langle H_i|$ $(i = 1, ?)$ and $\hat{\pi}_i = |V_i\rangle\langle V_i|$ $(i = 0, 2)$. The mode transformation from the interferometer input to these detector modes then means that $|H_i\rangle \propto |\phi_i\rangle$.

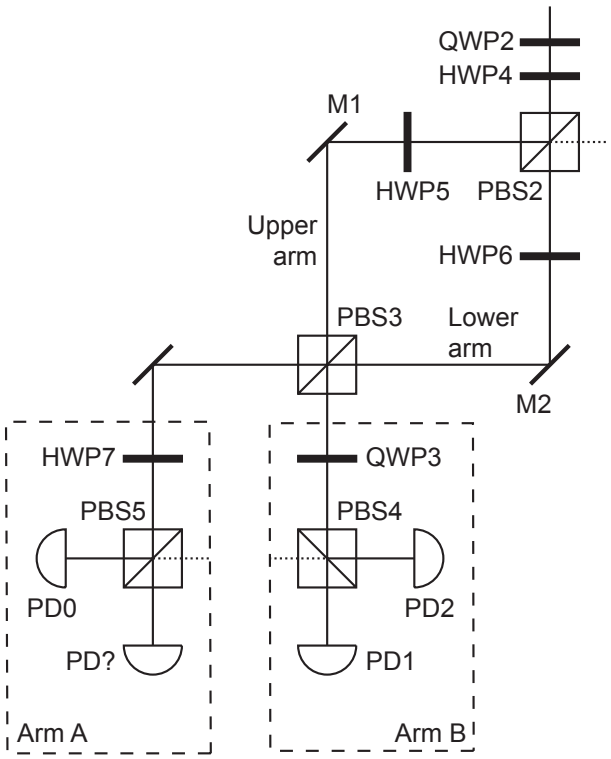

Fig. 2. Optical network to realise the maximum confidence measurement. PBS2–5 = polarising beamsplitters, HWP4–7 = zero-order half waveplates, QWP2–3 = zero-order quarter waveplates, PD0–2, PD? = amplified photodiodes. Dotted lines represent the vacuum inputs to PBS2,4-5.

3.2 Performing a general two outcome measurement

Before discussing the details of our measurement, it is useful to first consider how an arbitrary two outcome measurement on an input polarisation state may be implemented using linear optical elements. The simplest measurement of this kind is a von Neumann measurement which assigns the input state to one of two orthogonal modes, and may be implemented using a polarising beamsplitter [22]. More general two outcome measurements are possible however, and may be expressed in the POM formalism by means of a two-element POM $\{\hat{\Pi}_A, \hat{\Pi}_B\}$. Any such POM may be written

$$
\begin{aligned}
\hat{\Pi}_A &= \lambda_0|\lambda_0\rangle\langle\lambda_0| + \lambda_1|\lambda_1\rangle\langle\lambda_1|, \\
\hat{\Pi}_B &= (1-\lambda_0)|\lambda_0\rangle\langle\lambda_0| + (1-\lambda_1)|\lambda_1\rangle\langle\lambda_1| \qquad (20)
\end{aligned}
$$

where $0 \leq \lambda_0, \lambda_1 \leq 1$, and $|\lambda_0\rangle, |\lambda_1\rangle$ represent two orthonormal polarisation states. λ_0, λ_1 ($|\lambda_0\rangle, |\lambda_1\rangle$) are the eigenvalues (eigenkets) of $\hat{\Pi}_A$. Any such measurement may be implemented using an interferometer, as shown in our set-up. The measurement is completely defined by the probabilities of obtaining outcomes ω_A, ω_B for any given input state, and therefore any optical network realising these probabilities is a valid implementation of the POM.

It is assumed that the transmitted and reflected beams at each beamsplitter transit identical optical path lengths.

We also follow the convention that the orientations of the waveplates are specified by the angle the fast axis makes with the horizontal, measured anti-clockwise when viewed in the direction of propagation. The action of a half waveplate at an angle $A/2$ may then be expressed using Jones matrix notation [37] as

$$\hat{\Lambda}_{1/2}(A/2)\begin{pmatrix}|H\rangle\\|V\rangle\end{pmatrix}=\begin{pmatrix}\cos A & \sin A\\ \sin A & -\cos A\end{pmatrix}\begin{pmatrix}|H\rangle\\|V\rangle\end{pmatrix}. \quad (21)$$

Similarly, the action of the quarter waveplates in our apparatus, which are all oriented at either $\pm 45°$, may be expressed

$$\hat{\Lambda}_{1/4}(\pm 45°)\begin{pmatrix}|H\rangle\\|V\rangle\end{pmatrix}=\frac{1}{\sqrt{2}}\begin{pmatrix}1 & \pm i\\ \pm i & 1\end{pmatrix}\begin{pmatrix}|H\rangle\\|V\rangle\end{pmatrix}. \quad (22)$$

For simplicity, in this discussion we will consider pure input states, and assume for the moment that PBS2-3 transmit $|\lambda_0\rangle$ and reflect $|\lambda_1\rangle$. Thus for any given input state $|\Psi\rangle$, the components along $|\lambda_0\rangle$ and $|\lambda_1\rangle$ are separated at PBS2. HWP5-6 are used to rotate the polarisations in each arm, so that the magnitude of $|\lambda_0\rangle$ in the lower arm, and $|\lambda_1\rangle$ in the upper arm are reduced by factors $\lambda_0^{1/2}$, $\lambda_1^{1/2}$ respectively. Thus HWP5 should be oriented at $\gamma_0/2 = \arccos(\lambda_0^{1/2})/2$ and HWP6 at $\gamma_1/2 = \arccos(\lambda_1^{1/2})/2$. The polarisations are then recombined at PBS3. Thus, the input state

$$|\Psi\rangle = a_0|\lambda_0\rangle + a_1|\lambda_1\rangle \quad (23)$$

where $|a_0|^2 + |a_1|^2 = 1$, evolves to

$$\begin{aligned}|\Psi\rangle &\rightarrow a_0|\lambda_{0L}\rangle + a_1|\lambda_{1U}\rangle\\ &\rightarrow a_0(\lambda_0^{1/2}|\lambda_{0L}\rangle + (1-\lambda_0)^{1/2}|\lambda_{1L}\rangle)\\ &\quad +a_1((1-\lambda_1)^{1/2}|\lambda_{0U}\rangle - \lambda_1^{1/2}|\lambda_{1U}\rangle)\\ &\rightarrow a_1 e^{i\phi}(1-\lambda_1)^{1/2}|\lambda_{0B}\rangle + a_0(1-\lambda_0)^{1/2}|\lambda_{1B}\rangle\\ &\quad +a_0\lambda_0^{1/2}|\lambda_{0A}\rangle - a_1 e^{i\phi}\lambda_1^{1/2}|\lambda_{1A}\rangle \end{aligned} \quad (24)$$

at PBS2, HWP5-6, PBS3 respectively, where we have allowed for a phase ϕ to be introduced between the arms of the interferometer. The subscripts U, L refer to the upper and lower arms of the interferometer, while the subscripts A, B refer to the output arms A and B, as shown in Figure 2. The probability that the photon is found in output arm A or B is given by the modulus squared of the amplitude of the state in each arm, and may be written:

$$\begin{aligned}P(A) &= |a_0|^2\lambda_0 + |a_1|^2\lambda_1\\ P(B) &= |a_0|^2(1-\lambda_0) + |a_1|^2(1-\lambda_1).\end{aligned} \quad (25)$$

Thus the measurement $\{\hat{\Pi}_A, \hat{\Pi}_B\}$ is realised by this apparatus. Note that, perhaps surprisingly, the probabilities are independent of the phase of the interferometer, which only affects the polarisation of the output states, and not their magnitude. Any more complicated measurement may be realised as a series of measurements such as this one. This design is similar to that of Ahnert and Payne [38], but has the advantage of requiring fewer optical elements, and thus is easier to implement.

3.3 Experimental design

In our set-up, $\hat{\Pi}_A = \hat{\Pi}_? + \hat{\Pi}_0$, $\hat{\Pi}_B = \hat{\Pi}_1 + \hat{\Pi}_2$. The operator $\hat{\Pi}_A$ is:

$$\hat{\Pi}_A = \frac{1}{3}(\hat{\mathrm{I}} + 2(1-\tan^2\theta)|R\rangle\langle R| + \tan\theta(|R\rangle\langle L| + |L\rangle\langle R|)). \quad (26)$$

so that

$$\hat{\Pi}_A\begin{pmatrix}|R\rangle\\|L\rangle\end{pmatrix}=\begin{pmatrix}1-\frac{2}{3}\tan^2\theta & \frac{1}{3}\tan\theta\\ \frac{1}{3}\tan\theta & \frac{1}{3}\end{pmatrix}\begin{pmatrix}|R\rangle\\|L\rangle\end{pmatrix}. \quad (27)$$

Diagonalising this gives

$$\begin{aligned}\lambda_{0,1} &= (6\cos^2\theta)^{-1}(1+3\cos 2\theta \pm \sqrt{1+3\cos^2 2\theta})\\ |\lambda_0\rangle &= \cos\alpha|R\rangle + \sin\alpha|L\rangle\\ |\lambda_1\rangle &= -\sin\alpha|R\rangle + \cos\alpha|L\rangle,\end{aligned} \quad (28)$$

where $\cos 2\alpha = 2\cos 2\theta/\sqrt{1+3\cos^2 2\theta}$. The polarising beamsplitters in our experiment transmit horizontal polarisation, $|H\rangle$ and reflect vertical polarisation $|V\rangle$. Thus QWP2 (at 45°) and HWP4 (at $\alpha/2$) are used to perform a unitary transformation from the $|\lambda_0\rangle, |\lambda_1\rangle$ basis to the $|H\rangle, |V\rangle$ basis. It is easily verified by comparison of the matrix representations in the $|H\rangle, |V\rangle$ basis that up to an overall phase factor

$$\hat{\Lambda}_{1/2}(\alpha/2)\hat{\Lambda}_{1/4}(45°) = |H\rangle\langle\lambda_0| - |V\rangle\langle\lambda_1|. \quad (29)$$

Following the same reasoning as above we can see that the interferometer in our set-up transforms the input polarisation state $|\Psi\rangle$ as follows

$$\begin{aligned}|\Psi\rangle \rightarrow \big(&-e^{i\phi}(1-\lambda_1)^{1/2}|H_L\rangle\langle\lambda_1| + (1-\lambda_0)^{1/2}|V_L\rangle\langle\lambda_0|\\ &+\lambda_0^{1/2}|H_U\rangle\langle\lambda_0| + e^{i\phi}\lambda_1^{1/2}|V_U\rangle\langle\lambda_1|\big)|\Psi\rangle.\end{aligned} \quad (30)$$

The two desired outcomes in each arm are then realised by setting HWP7 to $\beta/2$ and QWP3 to 45°, where $\cos 2\beta = (3\cos 2\theta - 1)/\sqrt{1+3\cos^2 2\theta}$. Note that the phase of the interferometer, which is set to π radians in our apparatus, determines the polarisation of the output state in each arm of the interferometer, and therefore does affect these results. The input state is therefore now transformed to

$$\begin{aligned}|\Psi\rangle \rightarrow \big(&1/\sqrt{2}|H_B\rangle((1-\lambda_1)^{1/2}\langle\lambda_1| + i(1-\lambda_0)^{1/2}\langle\lambda_0|)\\ &+1/\sqrt{2}|V_B\rangle(i(1-\lambda_1)^{1/2}\langle\lambda_1| + (1-\lambda_0)^{1/2}\langle\lambda_0|)\\ &+|H_A\rangle(\lambda_0^{1/2}\cos\beta\langle\lambda_0| - \lambda_1^{1/2}\sin\beta\langle\lambda_1|)\\ &+|V_A\rangle(\lambda_0^{1/2}\sin\beta\langle\lambda_0| + \lambda_1^{1/2}\cos\beta\langle\lambda_1|)\big)|\Psi\rangle.\end{aligned} \quad (31)$$

After PBS4-5, the $|H_B\rangle, |V_B\rangle$ components can reach photodetectors PD1, PD2 respectively, while the $|H_A\rangle, |V_A\rangle$ components reach PD? and PD0. Finally, a little algebra confirms that the action of the entire apparatus on the input state may be expressed as follows

$$\begin{aligned}|\Psi\rangle \rightarrow &|PD1\rangle\big(1/\sqrt{3}(\tan\theta\langle R| + e^{-2\pi i/3}\langle L|)|\Psi\rangle\big)\\ &+|PD2\rangle\big(1/\sqrt{3}(\tan\theta\langle R| + e^{2\pi i/3}\langle L|)|\Psi\rangle\big)\\ &+|PD?\rangle(1-\tan^2\theta)^{1/2}\langle R|\Psi\rangle\\ &+|PD0\rangle\big(1/\sqrt{3}(\tan\theta\langle R| + \langle L|)|\Psi\rangle\big).\end{aligned} \quad (32)$$

where the photodetector state $|\mathrm{PD}i\rangle$ represents the detection of a photon at PDi. Thus

$$\begin{aligned} P(\omega_1|\Psi) &= (3\cos^2\theta)^{-1}|\langle\phi_1|\Psi\rangle|^2 \\ P(\omega_2|\Psi) &= (3\cos^2\theta)^{-1}|\langle\phi_2|\Psi\rangle|^2 \\ P(\omega_?|\Psi) &= (1-\tan^2\theta)|\langle R|\Psi\rangle|^2 \\ P(\omega_0|\Psi) &= (3\cos^2\theta)^{-1}|\langle\phi_0|\Psi\rangle|^2, \end{aligned} \tag{33}$$

as required, and the apparatus realises the desired measurement.

3.4 Experimental details

The maximum confidence measurement outlined above was performed for 10 values of the parameter θ, ranging from 0° to 45° in 5° steps. The apparatus used in our experiment is shown in Figure 3. The light source was an 810 nm laser diode (Laser 2000 PPMT model) run in CW mode, with a full width half maximum bandwidth of 0.88 nm and maximum power output of 20 mW. This was coupled into a single mode fibre to act as a spatial filter and ensure a well-controlled Gaussian spatial mode along the beam path. The output beam from the fibre was collimated using an aspheric lens. This beam was initially sent through a zero-order half waveplate (HWP1) followed by a polarising beamsplitter (PBS1) to provide clean horizontal input polarisation and to act as a variable attenuator.

Three waveplates were used to prepare each of the input states in turn. HWP2 was oriented at $\theta/2 - 45°$, QWP1 at $-45°$ for all input states, and HWP3 at $-\delta/4$ where $\delta = 0, 120°, -120°$ for $|\Psi_0\rangle, |\Psi_1\rangle$ and $|\Psi_2\rangle$ respectively. Again by comparing the matrix representation in the $|H\rangle, |V\rangle$ basis, it may be shown that

$$\begin{aligned} &\hat{\Lambda}_{1/2}(-\delta/4)\hat{\Lambda}_{1/4}(-45°)\hat{\Lambda}_{1/2}(\theta/2-45°) = \\ &(\cos\theta|R\rangle + e^{i\delta}\sin\theta|L\rangle)\langle H| + (\sin\theta|R\rangle - e^{i\delta}\cos\theta|L\rangle)\langle V|, \end{aligned} \tag{34}$$

and therefore that this combination produces the desired input state when acting on the input $|H\rangle$. Thus θ was set for each of the input states using HWP2, while the phase was set using HWP3. This arrangement allowed the input to be switched easily between the three input states $|\Psi_{0,1,2}\rangle$ by moving only one waveplate (HWP3).

In the measurement section of our apparatus, mirror M1 was mounted on a precision translation stage (Melles Griot Nanomax-TS 17MAX303), allowing the relative phase between the arms of the interferometer to be accurately varied. In order to minimise phase fluctuations, the interferometer was shielded from air currents by a box, and, when operating in Mach-Zender configuration, the visibility of the interference fringes were regularly measured to be better than 99% over a period of at least 10 minutes. It was also ascertained that the phase could be adjusted over a range greater than 2π radians without affecting the quality of the interference fringes. The phase could be most accurately controlled by adjusting the horizontal translation axis approximately parallel to the face of M1 (to give much smaller changes in the position of M1 for a given rotation of the adjustment knob than was possible using the translation axis perpendicular to the mirror face); therefore an extension was made for this adjuster to allow the phase to be set from outside the box containing the interferometer, minimising any disturbance to the interferometer during phase adjustments.

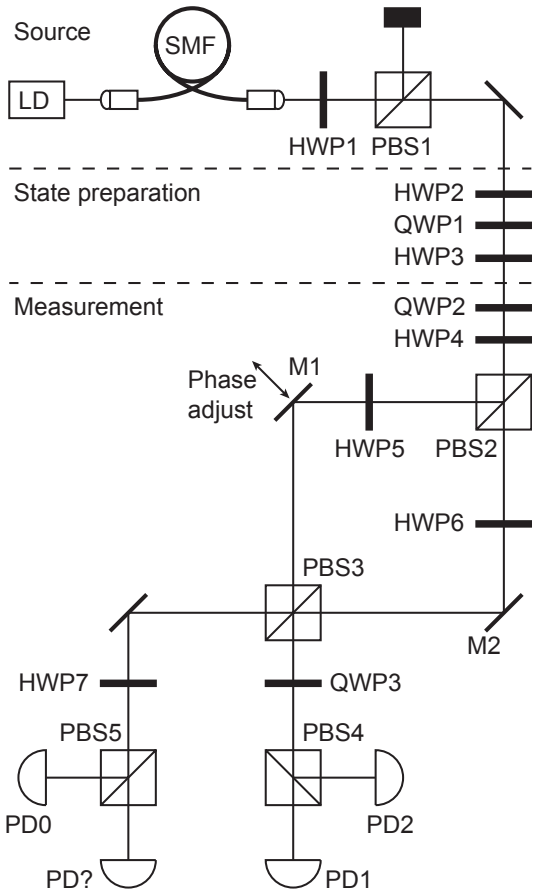

Fig. 3. Optical network to realise the maximum confidence measurement. LD = Laser diode, SMF = single mode fibre, PBS1–5 = polarising beamsplitters, HWP1–7 = zero-order half waveplates, QWP1–3 = zero-order quarter waveplate, PD0–2, PD? = amplified photodiodes [27].

The photodetectors used were amplified photodiodes (Thorlabs PDA520-EC) whose linearity and relative calibration were measured over the relevant range of incident power to be within 0.1% and 2.5% respectively. The output voltages of the four photodetectors were displayed and recorded using a digital oscilloscope (LeCroy Wavepro 7100). HWP1 was rotated to attenuate the power in the transmitted arm of PBS1 to keep the photodetectors within their linear response range. All the waveplates used were calibrated to within 0.1° and were measured to preserve the purity of the polarisation to better than 1:2000. The waveplates were held in precision mounts that allowed the angle of the optic axes to be set to within 0.1° with a repeatability of 0.1°. The extinction ratios of the beamsplitters were measured to be approximately 1:200.

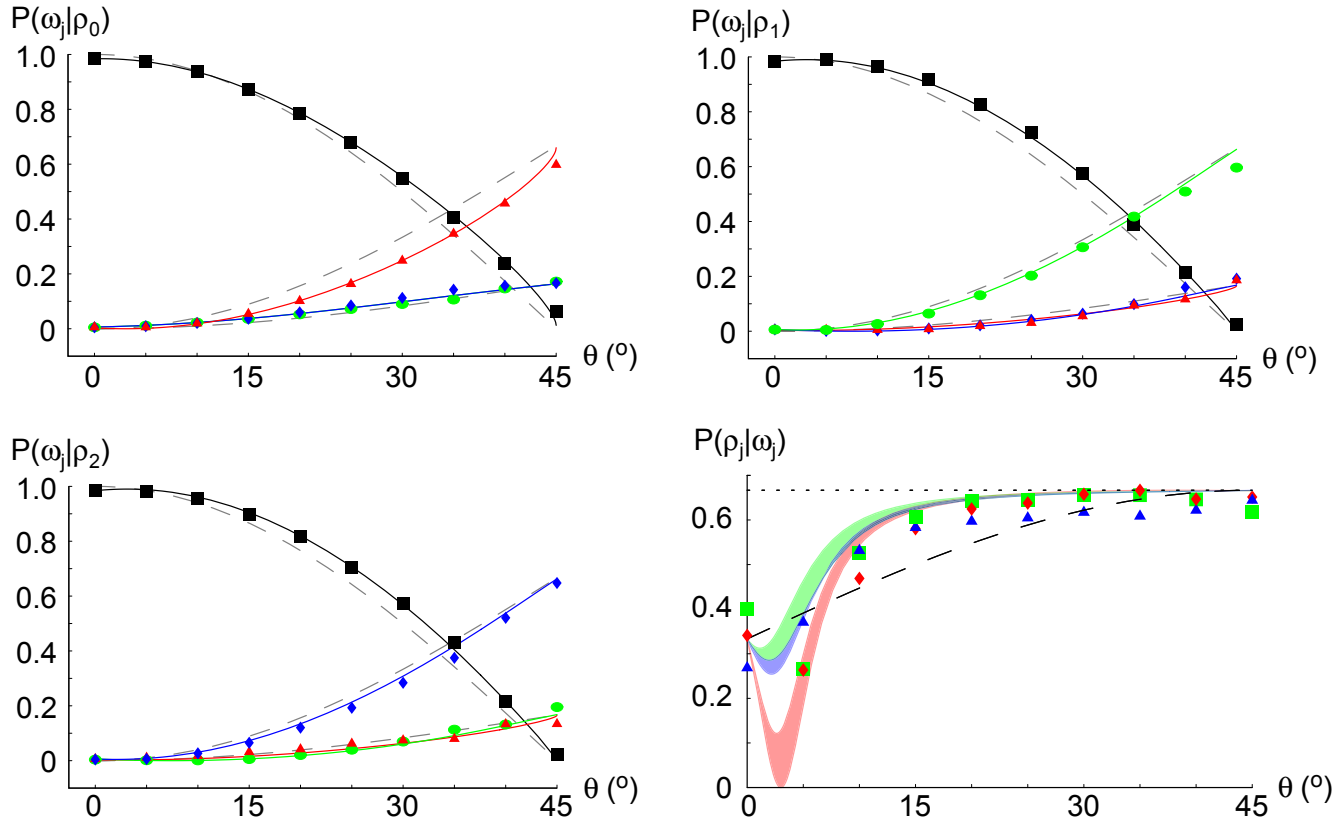

Fig. 4. (Colour online) Graphs show experimental results for the normalised voltages at each detector (registering output result ω_j) as a function of θ for input state: $|\Psi_0\rangle, |\Psi_1\rangle$ (top, l-r); $|\Psi_2\rangle$, and the confidence figure of merit calculated from these results (bottom l-r). Also shown are the theoretical predictions without error (grey dashed lines), and those of a non-ideal model which takes into account the errors introduced at beamsplitters PBS2 and PBS3 (coloured solid lines). Points correspond to the experimental results, with red triangles, black squares, green circles, blue diamonds corresponding to PD0, PD?, PD1, PD2 respectively. In the last plot red diamonds, green squares and blue triangles correspond to states $|\Psi_0\rangle, |\Psi_1\rangle, |\Psi_2\rangle$ respectively, and the lines indicate the confidence figure of merit for both the maximum confidence (dotted) and minimum error (dashed) measurement strategies. The data show a clear improvement of the state discrimination over the minimum error case. The shaded regions indicate the range of values consistent with the non-ideal model, which is explained fully in the text. Experimental errors, due to fluctuations in the measured voltages, are smaller than the size of the data points.

For the intended measurement, the probability of obtaining outcome $\omega_j, j = 0, 1, 2$, given input state $\hat{\rho}_i, i = 0, 1, 2$ may be expressed

$$P(\omega_j|\rho_i) = (3\cos^2\theta)^{-1}|\langle\phi_j|\Psi_i\rangle|^2 = (1-\cos 2\theta)\left(\frac{1}{6}+\frac{1}{2}\delta_{ij}\right) \quad (35)$$

where δ_{ij} is the Kroeneker delta. Thus the two results for which $j \neq i$ have the same probability of occurrence, as expected from the symmetry of the measurement. When the apparatus was set up to perform the measurement, this property was used to set the phase of the interferometer. In practice, at each value of θ, the state $|\Psi_1\rangle$ was input, and the phase of the interferometer was set by adjusting the position of M1 to minimise the difference between the outputs at detectors PD0 and PD2. Once the phase was set, it was possible to cycle quickly through the three input states by rotating HWP3. The output voltages were recorded for 10 seconds for each input state. These data were then averaged, and then normalised by dividing by the total voltage recorded at all detectors for each input state, so that the data could be interpreted as the probability that input state $\hat{\rho}_i$ gives result ω_j. The measurement outcomes depend only on the second order field correlation functions of the input light, as we look at the outputs of individual detectors, and not correlations between them. Thus there is no difference in the results for a one photon input or for classical light. What we are discriminating is the relative (complex) amplitudes of beams in two input modes — the two orthogonal polarisations. In the case of weak classical light, this can be interpreted as the relative probability amplitudes of a single photon distributed between the two modes.

4 Results

The results of our experiment [27] are shown in Figure 4. The first three graphs show the normalised voltages at

each detector for each input state $|\Psi_0\rangle, |\Psi_1\rangle, |\Psi_2\rangle$. The theoretical probabilities of obtaining outcome $\omega_j, j = 0, 1, 2$ given input state $\hat{\rho}_i$ were given above in equation (35). The probability of obtaining outcome $\omega_?$, as discussed previously, is the same for all three input states in each set, and equal to $\cos 2\theta$. These theoretical predictions are shown alongside our experimental results. These data were then used to calculate the confidence figure of merit, shown in the fourth graph in Figure 4. In the experimental implementation the confidence figure of merit represents the proportion of the voltage recorded at detector PDi, $i = 0, 1, 2$, which was due to the corresponding input state $\hat{\rho}_i$. Again the theoretical value of $2/3$ is also shown on this graph. For comparison purposes we have also shown the confidence achieved by the theoretically optimal minimum error measurement. Experimental errors are due to fluctuations in the voltages over the 10 seconds for which they were recorded, and are smaller than the size of the data points.

Modelling of the errors due to the different components of our apparatus showed that the largest errors were associated with the beamsplitters used in the interferometer, PBS2 and PBS3. Ideally, these beamsplitters transmit all incident $|H\rangle$ and reflect all incident $|V\rangle$. In modelling the error, we assumed that 0.5% of the intensity of the incident light leaks into the wrong output port. This level of error is based on our calibration data, and the polarising beamsplitters PBS2 and PBS3 are thus modelled by the following operator:

$$\begin{aligned} PBS = &|H_L\rangle(ie^{-i\chi}\sqrt{0.005}\langle H_L| + \sqrt{0.995}\langle H_U|) \\ &+|V_L\rangle(\sqrt{0.995}\langle V_L| + ie^{i\chi}\sqrt{0.005}\langle V_U|) \\ &+|H_U\rangle(\sqrt{0.995}\langle H_L| + ie^{i\chi}\sqrt{0.995}\langle H_U|) \\ &+|V_U\rangle(ie^{-i\chi}\sqrt{0.005}\langle V_L| + \sqrt{0.995}\langle V_U|) \quad (36) \end{aligned}$$

where χ is the phase introduced between the intended and erroneous components. No phase information was available, and this was therefore left as a parameter in our model. The form of the above operator is chosen so that for the input in each arm the reflected and transmitted components have the same phase, both for the intended and erroneous components.

It was found that the predictions of the non-ideal model for the probabilities of obtaining each outcome gave best agreement with our data for $\chi = \pi/2$, corresponding to the case in which all the transmission and reflection coefficients are real. These predictions are shown alongside our results in Figure 4. However there is little change in the predictions of the non-ideal model for these probabilities for $\pi/3 \leq \chi \leq 2\pi/3$. The predictions for the confidence figure of merit do vary within this range however, and the full range of values for which the non-ideal model is consistent with our raw data are shown. The remaining differences between the model and our experimental results are due to second order effects such as errors in the waveplates and in setting the phase of the interferometer. Residual errors may also be due to non-pure input states arising from the bandwidth of the input being greater than that of the detectors.

The results show a clear improvement in the confidence figure of merit over the corresponding minimum error measurement. This is most evident in the range $10^\circ \leq \theta \leq 30^\circ$. For θ larger than this range, this figure of merit is comparable for the two strategies. For θ smaller than this range, the input states are very close together, and distinguishing between them is more difficult. Experimental errors are therefore more significant in this region, as can be seen from our non-ideal theory plot.

5 Conclusion

In the problem of discriminating between non-orthogonal quantum states, the maximum confidence measurement allows us to be as confident as possible that if we infer from the measurement result that a given state was present, that state was indeed present. This confidence is maximised for all states in a given set, independent of the frequency with which any given result occurs. Therefore maximising the confidence measure does not define a unique strategy. Moreover, it is sometimes necessary to include an inconclusive outcome in order to form a complete measurement. The maximum confidence measurement has the advantage that it is possible to write down an analytic solution for the optimal POM elements for an arbitrary set of states. This is not usually possible for other strategies.

We have demonstrated a maximum confidence measurement experimentally for a set of three equiprobable symmetric polarisation states. Our results show an improvement in the confidence figure of merit over the optimal minimum error measurement for the same set.

This work was supported by the EPSRC, and by the Synergy fund of the Universities of Glasgow and Strathclyde. PJM acknowledges support by the National Science Foundation through its Information Technology Research (ITR) program, grant number PHY-0219460, via a collaboration with the University of Oregon. IAW acknowledges support by the DARPA QuIST programme via a collaboration with Princeton University. We thank E. Riis for helpful discussions. IAW thanks R. Kosut and H. Rabitz for introducing him to the ideas of optimal detection measurements and for useful conversations on quantum state discrimination. SC and SMB would like to thank J. Jeffers, E. Andersson and C. Gilson with whom we have enjoyed working on state discrimination problems.

References

1. C.H. Bennett, G. Brassard, *Proceedings of the IEEE Conference on Computers, Systems and Signal Processing* (Bangalore, India, 1984), p. 175
2. C.H. Bennett, Phys. Rev. Lett. **68**, 3121 (1992)
3. C.A. Fuchs, Phys. Rev. Lett. **79**, 1162 (1997)
4. For a review of quantum state discrimination see A. Chefles, Contemp. Phys. **41**, 401 (2000)
5. C.W. Helstrom, *Quantum Detection and Estimation Theory* (Academic, New York, 1976)
6. A.S. Holevo, J. Multivariate Anal. **3**, 337 (1973)

7. H.P. Yuen, R.S. Kennedy, M. Lax, IEEE Trans. Inf. Theory **IT-21**, 125 (1975)
8. I.D. Ivanovic, Phys. Lett. A **123**, 257 (1987); D. Dieks, Phys. Lett. A **126**, 303 (1988); A. Peres, Phys. Lett. A **128**, 19 (1988)
9. A. Peres, D. Terno, J. Phys. A **31**, 7105 (1998)
10. A. Chefles, Phys. Lett. A **239**, 339 (1998)
11. S. Croke, E. Andersson, S.M. Barnett, C.R. Gilson, J. Jeffers, Phys. Rev. Lett. **96**, 070401 (2006)
12. E.B. Davies, IEEE Trans. Inf. Theory **IT-24**, 596 (1978)
13. M. Sasaki, S.M. Barnett, R. Josza, M. Osaki, O. Hirota, Phys. Rev. A **59**, 3325 (1999)
14. S.M. Barnett, C.R. Gilson, M. Sasaki, J. Phys. A **34**, 6755 (2001)
15. K. Hunter, E. Andersson, C.R. Gilson, S.M. Barnett, J. Phys. A **36**, 4159 (2003)
16. R.L. Kosut, I.A. Walmsley, Y.C. Eldar, H. Rabitz, e-print `arXiv:quant-ph/0403150`
17. U. Herzog, J.A. Bergou, Phys. Rev. A **65**, 050305(R) (2002)
18. Y. Sun, J.A. Bergou, M. Hillery, Phys. Rev. A **66**, 032315 (2002)
19. J.A. Bergou, U. Herzog, M. Hillery, Phys. Rev. Lett. **90**, 257901 (2003)
20. For a review see S.M. Barnett, Quantum Inf. Comput. **4**, 450 (2004)
21. M. Mohseni, A.M. Steinberg, J.A. Bergou, Phys. Rev. Lett. **93**, 200403 (2004)
22. S.M. Barnett, E. Riis, J. Mod. Opt. **44**, 1061 (1997)
23. R.B.M. Clarke, V.M. Kendon, A. Chefles, S.M. Barnett, E. Riis, M. Sasaki, Phys. Rev. A **64**, 012303 (2001)
24. B. Huttner, A. Muller, J.D. Gautier, H. Zbinden, N. Gisin, Phys. Rev. A **54**, 3783 (1996)
25. R.B.M. Clarke, A. Chefles, S.M. Barnett, E. Riis, Phys. Rev. A **63**, 040305 (2001)
26. J. Mizuno, M. Fujiwara, M. Akiba, S.M. Barnett, M. Sasaki, Phys. Rev. A **65**, 012315 (2002)
27. P.J. Mosley, S. Croke, I.A. Walmsley, S.M. Barnett, Phys. Rev. Lett. **97**, 193601 (2006)
28. G.M. D'Ariano, M.F. Sacchi, J. Kahn, Phys. Rev. A **72**, 032310 (2005)
29. A. Peres, *Quantum Theory: Concepts and Methods* (Kluwer Academic Publishers, Dordrecht, 1993)
30. G. Jaeger, A. Shimony, Phys. Lett. A **197**, 83 (1995)
31. M. Ban, K. Kurokawa, R. Momose, O. Hirota, Int. J. Theor. Phys. **36**, 1269 (1997)
32. S.M. Barnett, Phys. Rev. A **64**, 030303 (2001)
33. E. Andersson, S.M. Barnett, C.R. Gilson, K. Hunter, Phys. Rev. A **65**, 044307 (2002)
34. Y.C. Eldar, G.D. Forney, IEEE Trans. Inf. Theory **IT-47**, 858 (2001)
35. P. Hausladen, W.K. Wooters, J. Mod. Opt **41**, 2385 (1994)
36. M. Born, E. Wolf, *Principles of Optics* (Pergamon, Oxford, 1987)
37. E. Hecht, *Optics*, 2nd edn. (Addison-Wesley, Reading, MA, 1987)
38. S.E. Ahnert, M.C. Payne, Phys. Rev. A **71**, 012330 (2005)